

Re-evaluation of plate-fin heatsink natural convection correlations for sideways and 3D inclinations

Mehdi Mehrtash<sup>1\*</sup>

<sup>1</sup> Energy Systems Engineering, Atilim University, Ankara 06830, Turkey

## **Abstract**

The common orientations of the plate-fin heat sink for natural convection cooling of electronics are vertical and upward-facing horizontal. However, depending on various use scenarios, the heat sink may be inclined, intentionally or otherwise. In our previous papers concerning this subject, the author proposed a set of correlations for plate-fin heat sinks covering all inclination angles backward and forward (pitch rotation) from the vertical position of the heat sink. The set was based on a series of computational simulations with a validated model. At the time, tilting the heat sink sideways (roll rotation) was not considered. In the present study, though, the sideways inclination of the plate-fin heat sinks is simulated using our previous model only by adjusting the direction of the gravitational acceleration vector, thus requiring no additional validation. It is determined that the previously proposed correlation is valid up to 80° sideways inclinations of the heat sink. Interesting flow structures are observed when the heat sink is tilted 90° sideways. Furthermore, it is demonstrated that the correlation surprisingly remains valid if the heat sink is simultaneously rotated in both axes (pitch and roll).

## **Introduction**

---

\* Corresponding author. Energy Systems Engineering, Atilim University, 06830, Ankara, Turkey.

Tel.: +90 312 586 8790; E-mail address: mehdi.mehrtash@atilim.edu.tr

Developing effective thermal management systems for electronics is proving to be a challenge due to the compact and ever-shrinking nature of modern electronic devices. Additionally, increased device portability calls for an evaluation of the relationship between the orientation of the device and the thermal performance of the natural convection cooling solution. One of the most commonly used solutions is the application of plate-fin heat sinks [1-4]. While other solutions may respond well to natural convection in any mounting orientation, the plate-fin heat sink has a strong orientation dependency and performs better when installed vertically or upward-facing horizontally [5]. However, due to a variety of system-related constraints, such as the shortage of available space or the absence of any vertical or horizontal surfaces in the design, these two orientations may not be feasible. Apart from this, at certain orientations, due to the diminishing effectiveness of the fin array, major increases in the junction temperatures of the electronics may occur, resulting in device failures. Overheating may also take place due to the tilting of the originally horizontal or vertical plate-fin heat sink attached to the device as a result of its rotation during use. Natural convection-based cooling strategies applied to laptop computers [4], flat panel displays [6], LED devices [7,8], vehicle onboard chargers [9], and photovoltaic panels [10-13] are sensitive to inclinations of the heat sink, motivating the present work on the investigation of 3D inclinations of plate-fin heat sinks.

The plate-fin heat sink consists of an array of parallel plates attached to a base. When the heat sink is vertically oriented, the channels between the adjacent fins act as minimal resistance flow paths for the fluid to rise freely with the buoyancy force due to heating by the heat sink surface. Due to the ease of flow, the heating fluid moves away from the hot surface and is replaced with cooler fresh fluid. However, in an inclined configuration, the buoyancy force is not in the direction of the channel. For vertically oriented plate fins with narrow spacing, the velocity

profile is symmetric between the plates and the boundary layers on the plates interact with each other, thus attaining a fully developed profile. Yet again, the asymmetric velocity profile is a particular challenge when working with inclined parallel plates. In this respect, the literature states that when the inclination angle is low, the influence on the flow structure between two parallel plates is minimal [14]. Furthermore, various correlations have been proposed for inclined channels, applicable across a broad range of inclination angles, ranging from  $0^\circ$  to  $85^\circ$  [15,16]. Similarly, for closely spaced plates as in plate-fin heat sinks, it is plausible to assume that the viscous forces are strong enough to repel any significant asymmetry. Through the simulation of various heat sink configurations, we aim to investigate this issue in the present study. The primary objective of our research is to establish correlations that apply to all plate-fin heat sink orientations, including sideways and 3D inclinations.

The literature presents several studies focusing on the impact of rotation on natural convection from heat sinks. For instance, Starner and McManus [17] conducted experimental investigations on heated rectangular fin arrays positioned at  $0^\circ$ ,  $45^\circ$ , and  $90^\circ$  angles. Similarly, Leung and Probert [5] explored heat sink configurations with vertical fins on horizontal, horizontal fins on vertical, and vertical fins on vertical bases. Mittelman et al. [18] performed research on fin arrays that are oriented downward with inclinations of up to  $30^\circ$ . Shen et al. [8] conducted experimental and numerical analyses to evaluate the heat dissipation performance of the heat sink at eight different rotation angles:  $0^\circ$ ,  $45^\circ$ ,  $90^\circ$ ,  $135^\circ$ ,  $180^\circ$ ,  $225^\circ$ ,  $270^\circ$ , and  $315^\circ$ . In our previous works [1-3], we conducted a numerical investigation on plate-fin heat sinks for backward and forward inclinations. Each geometric parameter underwent rigorous examination to discern its influence on natural convection heat transfer rates. By utilizing the proposed correlations for vertical orientation and adjusting the body force using the cosine of the

inclination angle, we demonstrated the validity of these correlations for a wide range of forward and backward inclination angles. However, research is lacking in experimental or computational investigations on sideways-inclined plate-fin heat sinks. To bridge this gap, our study aims to comprehensively explore fluid flow and heat transfer characteristics in sideways-tilted heat sinks. Employing a methodology similar to previous work, we investigate the effect of inclination on heat sink performance, considering rotations about both length and width. Our primary objective is to establish correlations applicable to all plate-fin heat sink orientations, including sideways and 3D inclinations. Confirming the applicability of the correlation suggested in [1], we demonstrate its suitability for sideways-inclination angles from  $0^\circ$  to  $80^\circ$ . Ultimately, we validate the proposed correlation for cases where the heat sink is inclined both longitudinally and laterally. These findings promise to aid in designing heat sinks oriented at unconventional angles and predicting thermal performance under intentional or accidental inclinations.

### **Numerical model**

The numerical model is constructed based on an experimental setup described in [19], utilizing the same parameters to ensure consistency and accuracy. Fig. 1a shows the computational domain considered for the present numerical study consisting of an assembly placed in a cubical room of  $3\text{m}\times 3\text{m}\times 3\text{m}$ . The assembly includes a heat sink mounted on the front side of a heater plate with aerated concrete insulation on its backside (Fig. 1b). The rotation around the z-axis is defined as ‘roll’, and the rotation around the x-axis is defined as ‘pitch’, as shown in Fig. 1c. According to Fig. 1d, when the base plate tilts from  $0^\circ$  to  $90^\circ$ , the protruding fins shift from vertically oriented to horizontally oriented positions.

This study serves as a continuation of our previous research efforts, extending the investigation into sideways-tilted plate-fin heat sinks, thus building upon the foundation laid in

our earlier studies [1-3]. We employed the ANSYS Fluent solver to solve the continuity, momentum, and energy equations, supplemented by the surface-to-surface radiation model to account for radiative heat transfer. The flow regime is handled by the zero-equation turbulence model [20]. To minimize numerical uncertainties, we conducted a grid sensitivity analysis to ensure grid independence [21]. In our previous study [1], we calculated the average temperature of the heat sink surface and determined the radiative and convective heat transfer rates from the simulation results. Additionally, a parametric analysis of the vertical case was conducted, identifying optimal values of 11.75 mm for the fin spacing ( $S_{opt}$ ) and 250 mm for the heat sink length ( $L$ ) to minimize surface temperature. We proposed a correlation based on the analysis of the entire dataset for the Nusselt number in the vertical orientation derived from the simulations. We validated our simulation results using data from [19] and relevant literature ([17,22-24] for the vertical case and [17,18] for backward/forward inclined cases), ensuring the accuracy and reliability of our numerical model. For a detailed overview of our model validation processes and the impact of various parameters on the heat transfer rate of vertically oriented heat sinks, please refer to our previous work [1].

In this study, while maintaining the fin spacing and the fin length at the optimal values, a series of simulations are conducted by altering the fin height ( $H = 5$  mm, 15 mm, and 25 mm), heat input values ( $Q_{in} = 25$  W, 75 W, and 125 W), and the inclination angles ( $\psi = 10^\circ, 20^\circ, 30^\circ, 45^\circ, 60^\circ, 75^\circ, 80^\circ, \text{ and } 90^\circ$ ), in which the angle ( $\psi$ ) is defined with respect to the vertical y-axis. The direction of the gravitational acceleration ( $g$ ) vector on the x-y plane is modified to provide the required sideways-inclined orientation of the heat sink. With this approach, no further validation is necessary because the previously validated vertical model is employed throughout with only a change in the  $g$ -direction.

## Mathematical formulation

Based on the coordinate system presented in Fig.1,  $u$  and  $v$  represent the flow velocity in the  $x$ - and  $y$ -directions, respectively. The flow velocity in the  $z$ -axis is denoted with  $w$  and is treated as negligible. In sideways inclinations, the  $z$ -axis is always perpendicular to the direction of the gravitational field, which acts along the  $y$ -axis. This results in the gravitational source term appearing only in the  $x$ - and  $y$ -directions within the momentum equations. As a result, the following are the governing equations for this case study [1,5]:

*Continuity equation*

$$\frac{\partial u}{\partial x} + \frac{\partial v}{\partial y} = 0 \quad (1)$$

*x-momentum equation*

$$\rho u \frac{\partial u}{\partial x} + \rho v \frac{\partial u}{\partial y} = -\frac{dp}{dx} + \mu \left( \frac{\partial^2 u}{\partial x^2} + \frac{\partial^2 u}{\partial y^2} + \frac{\partial^2 u}{\partial z^2} \right) \quad (2)$$

*y-momentum equation*

$$\rho u \frac{\partial v}{\partial x} + \rho v \frac{\partial v}{\partial y} = -\frac{dp}{dy} + \mu \left( \frac{\partial^2 v}{\partial x^2} + \frac{\partial^2 v}{\partial y^2} + \frac{\partial^2 v}{\partial z^2} \right) + \rho g \beta \Delta T \quad (3)$$

*z-momentum equation*

$$\frac{\partial p}{\partial z} = 0 \quad (4)$$

*Energy equation*

$$\rho c_p u \frac{\partial T}{\partial x} + \rho c_p v \frac{\partial T}{\partial y} = \left( u \frac{dp}{dx} + v \frac{dp}{dy} \right) + k \left( \frac{\partial^2 T}{\partial x^2} + \frac{\partial^2 T}{\partial y^2} + \frac{\partial^2 T}{\partial z^2} \right) \quad (5)$$

The inclusion of two pressure gradient terms in the energy equation accounts for the impacts of buoyancy and gravitational forces, both of which significantly influence the flow dynamics

around the heat sink, depending on factors such as its orientation and the density gradients within the air.

To reach a dimensionless correlation Eqs. (1)-(5) should be non-dimensionalized. The coordinates in non-dimensional space are as follows:

$$X = \frac{x}{S} \quad Y = \frac{y}{L} \quad Z = \frac{z}{H} \quad (6)$$

The components of non-dimensional velocity can be expressed as

$$\mathcal{U} = \frac{u}{u'} \quad \mathcal{V} = \frac{v}{v'} \quad (7)$$

The velocity in the y-direction can be calculated by multiplying the density  $\rho$ , body force  $g$ , the volumetric expansion coefficient  $\beta$ , the temperature excess of air between two adjacent fins and the ambient  $(T - T_a)$ , and the channel cross-sectional area divided by dynamic viscosity  $\mu$ .

Velocity in y-direction can be non-dimensionalized by defining:

$$v' = \frac{\rho g \beta (T_w - T_a) S H}{\mu} \quad (8)$$

in which  $T_w$  represents the average heat sink temperature. To meet the requirements of the continuity equation in a dimensionless format:

$$\frac{v' \partial \mathcal{V}}{L \partial Y} = - \frac{u' \partial \mathcal{U}}{S \partial X} \quad i.e. \quad \frac{v'}{L} = \frac{u'}{S} \quad \text{thus} \quad u' = \left(\frac{S}{L}\right) v' \quad (9)$$

The temperature in non-dimensional form is:

$$\phi = \frac{T - T_a}{T_w - T_a} \quad (10)$$

Pressure in non-dimensional form is:

$$P = \frac{p}{\rho (u')^2} \quad (11)$$

Utilizing these definitions inside Eqs. (1)-(5), the non-dimensional form of governing equations can be obtained as follows:

*Continuity equation*

$$\frac{\partial u}{\partial X} + \frac{\partial v}{\partial Y} = 0 \quad (12)$$

*x-momentum equation*

$$u \frac{\partial u}{\partial X} + v \frac{\partial u}{\partial Y} = - \left(\frac{L}{S}\right)^2 \frac{dP}{dX} + \frac{\nu}{Su'} \left[ \left(\frac{S}{H}\right)^2 \frac{\partial^2 u}{\partial X^2} + \frac{\partial^2 u}{\partial Y^2} + \left(\frac{S}{L}\right)^2 \frac{\partial^2 u}{\partial Z^2} \right] \quad (13)$$

*y-momentum equation*

$$u \frac{\partial v}{\partial X} + v \frac{\partial v}{\partial Y} = - \frac{dP}{dY} + \frac{\nu}{Su'} \left[ \left(\frac{S}{H}\right)^2 \frac{\partial^2 v}{\partial X^2} + \frac{\partial^2 v}{\partial Y^2} + \left(\frac{S}{L}\right)^2 \frac{\partial^2 v}{\partial Z^2} \right] + \frac{\nu}{v'H} \quad (14)$$

*z-momentum equation*

$$\frac{\partial P}{\partial Z} = 0 \quad (15)$$

*Energy equation*

$$\begin{aligned} \frac{\nu}{Hu'} \left( u \frac{\partial \phi}{\partial X} + v \frac{\partial \phi}{\partial Y} \right) &= \frac{g\beta L}{c_p} \left( u \frac{dP}{dX} + v \frac{dP}{dY} \right) \\ &+ \frac{\nu k}{\rho c_p S H u'^2} \left[ \left(\frac{S}{H}\right)^2 \frac{\partial^2 \phi}{\partial X^2} + \frac{\partial^2 \phi}{\partial Y^2} + \left(\frac{S}{L}\right)^2 \frac{\partial^2 \phi}{\partial Z^2} \right] \end{aligned} \quad (16)$$

Dimensionless groups can be obtained by rearranging the terms in Eqs. (13)-(16) as:

$$\frac{\nu}{Su'} = \left( \frac{\nu}{Hu'} \right) \left( \frac{H}{S} \right) \quad (17)$$

$$\frac{\nu}{Hu'} = \frac{\nu}{H \left[ \frac{g\beta(T_w - T_a)SH}{\nu} \right] \left( \frac{S}{L} \right)} = \frac{1}{\left[ \frac{g\beta(T_w - T_a)S^3}{\nu^2} \right] \left( \frac{H}{S} \right) \left( \frac{H}{L} \right)} \quad (18)$$

$$\frac{\nu k}{\rho c_p S H u'^2} = \frac{1}{\left(\frac{H u'}{\nu}\right)^2 \left(\frac{S}{H}\right) \left(\frac{\mu c_p}{k}\right)} \quad (19)$$

Therefore, dimensionless groups are  $\Pi_1 = H/L$ ,  $\Pi_2 = S/H$ ,  $\Pi_3 = [g\beta(T_w - T_a)S^3]/\nu^2 \equiv Gr$ ,  $\Pi_4 = (\mu c_p)/k \equiv Pr$  and  $\Pi_5 = g\beta L/c_p$ . For small temperature variations, we can neglect  $\Pi_5$ . Combining  $\Pi_1$ ,  $\Pi_2$ , and  $\Pi_3$ , modified Grashof number can be defined as:

$$Gr' = Gr(H/L)^{m_1}(S/H)^{m_2} \quad (20)$$

According to [5] the most suitable power indices to correlate the data are  $m_1 = 1/2$  and  $m_2 = 1$ . Using these power indices in Eq. (20) results in the following equation:

$$\begin{aligned} Gr' &= \{[g\beta(T_w - T_a)S^3]/\nu^2\}(H/L)^{1/2}(S/H) \\ &= [g\beta(T_w - T_a)S^4]/[\nu^2(HL)^{1/2}] \end{aligned} \quad (21)$$

Even though in the present study the rotation plane is the x-y plane rather than the y-z plane (as in our previous attempt), the resultant modified Grashof number is the same as the one proposed in [1]. Accordingly, the Nusselt number correlation as a function of fin spacing takes the following form:

$$Nu_s \equiv \frac{hS}{k} = C(Gr'Pr)^n \quad (22)$$

To establish a correlation for the vertical scenario,  $Nu_s$  was plotted against  $Gr'Pr$  by utilizing the whole vertical orientation data set [1]. Using the form given in Eq. (22), the entire data was processed. Based on the power curve fit applied, the  $C$  coefficient and the power,  $n$ , were obtained as 0.252 and 1/3, respectively. Consequently, the suggested correlation in [1] is still applicable for the present study:

$$Nu_s = 0.252(Gr'Pr)^{1/3} \quad \text{for} \quad 250 < Gr'Pr < 10^6, \quad H \geq 15 \text{ mm} \quad (23)$$

For both forward and backward directions, it has been shown that the correlation for the vertical case can still be valid in  $-60^\circ \leq \theta \leq +80^\circ$  by only replacing  $Gr'$  with  $Gr' \cos(\theta)$ . The underlying premise of this approach is that the flow structure remains constant and that the only change is in the body force, which becomes  $\rho g \cos(\theta)$ . With the same rationale, provided that the flow structure stays constant, the vertical-case correlation, Eq. (23), is expected to be valid as well for sideways inclination by substituting  $Gr'$  with  $Gr' \cos(\psi)$ .

## Results and discussion

### *Velocity field for sideways inclination*

On a vertically oriented heat sink, gravity is in the same orientation with the plate fins; however, for heat sinks that are inclined, the buoyancy force components are both parallel and perpendicular to the plate fin surfaces. Compared to the vertical orientation, when the fins are inclined, the buoyancy force parallel to the surface decreases, resulting in a lower airflow velocity along the fin channels and a lower convection heat transfer. Fig. 2 demonstrates the flow dynamics over the heat sink with different inclination angles on the x-y plane in the case of  $H=25$  mm and  $Q_{in}=75$  W. The scale for the flow speed is the same for all of the subfigures, as illustrated in Fig. 2a.

Various buoyancy-driven flow configurations form as a result of heat sink orientation. Each orientation causes the formation of an upward flow, in which the air is drawn into the channels formed by two parallel fins, heats up as it moves through them, and then exits from the top edge. Eventually, all inclination angles result in the plume lining up in the direction of gravity. The plume forms at the top edge of the heat sink between the  $0^\circ$  and  $80^\circ$  range of inclination angles. The plume separation spot approaches the leading edge as the inclination angle increases; from  $80^\circ$  to  $90^\circ$ , this spot slides down until it reaches the center at  $90^\circ$  (Fig. 2f). As a result, at  $80^\circ$  and

higher inclination angles, the flow structure resembles that of the horizontal orientation ( $\psi = 90^\circ$ ) rather than the vertical one. When the fins are oriented at  $90^\circ$ , the buoyancy force along the surface and between the fins of a horizontal plate is close to zero and, hence, insignificant. As seen in Fig. 2f, the presence of longitudinal vortices is also detected as secondary motions (circulation zones) with an almost stagnant flow in the vicinity of the channel middle section. Due to its relatively low performance, the plate-fin array with a horizontal orientation is not a favorable configuration.

To assess the impact of the inclination angle on the flow characteristics inside the inter-fin gaps, the velocity vectors are presented on the y-z plane cut through the middle channel in Fig. 3. As the inclination angle increases, the air velocity decreases continuously. For large inclination angles, the flow comes to a near standstill caused by an increase in flow resistance. The generated buoyancy flow between fins is so small that the air around the fin bases is essentially motionless, suggesting that when heat sinks function in an unfavorable direction, air movement and heat transfer are significantly impeded.

To understand the behavior displayed in Fig. 2f and Fig. 3f, the flow dynamics in the inter-fin gaps for the horizontally oriented plate-fins are further examined on the x-z plane. In Fig. 4, the streamline plots are taken at an angle of  $\psi = 90^\circ$  for each of the recirculating sections at the center of each channel for three different fin height cases. The primary air stream is directed upward and parallel to the vertical base, and only a minor portion of the main flow is entrained into the spaces between the adjacent fins. The natural convection flow is blocked from entering the channels by the fins. The primary flow is obstructed, but it is still able to move through the initial inter-fin gap. Although obstruction occurs less as the air moves past the succeeding channels, the fin tips still disturb the main flow, causing vortices to trail after the fins. The

buoyancy force leads to the 3D cell structures inside the inter-fin gaps. The cellular pattern is formed by the movement of the cooler fluid toward the hot surface to maintain mass conservation and replaces the departed fluid. As the fin height increases, so does the obstruction of the flow, thereby preventing the air present in the surrounding colder areas from entering the inter-fin gaps and resulting in reduced velocities in the flow field. This enhances the prospect of a distinct convection cell forming between each pair of neighboring fins, leading to a lower heat transfer rate in comparison to a vertically oriented heat sink. In the space between each pair of parallel fins at a fin height of 5 mm, only a single, very small vortex is formed. When the fin height is increased to 15 mm, less air from the mainstream enters the gap. Two counter-rotating vortices are formed in the inter-fin channels: one near the fin tip and another practically stagnant toward the base. The size of the lower vortex is important for heat transfer because it promotes fluid mixing near the base wall, which is the primary heat transfer surface. When the fin height is changed to 25 mm, despite increasing the size of both vortices around the fin tip and base, less flow enters the inter-fin channels compared to the 15mm case. As a consequence of the formation of longitudinal vortices and ineffective use of the heat sink surface, the heat transfer rate drops considerably. These observations are in agreement with the ones provided in [8].

#### *Inclination angle dependence of $u$ , $v$ , and $w$*

To quantify the influence of the inclination angle on the velocity field, the air velocity variation in three directions ( $x$ ,  $y$ ,  $z$ ) inside the center channel of the heat sink is extracted from the simulation results and presented in Fig. 5. The precise location of the line, over which the velocity magnitudes are obtained, is superimposed on each figure. The changes are illustrated over the line positioned in the mid-width and mid-height of the channel with respect to the fin length. The selected fin height is 25 mm and, as such, the line is 12.5 mm above the base plate.

The negative values indicate the flow in the opposite direction with respect to the corresponding axis.

The rate of change of  $u$  (velocity in the x-direction) is high at the inlet and exit of the channel, while low in the middle (see Fig. 5a). As the inclination angle increases, the velocity gradients in the channel inlet and exit portions increase. Due to the stronger buoyancy force at the top of the channel, the velocity profile is not symmetrical against the mid-point. Compared to other inclination angles,  $\psi = 90^\circ$  shows a substantial difference in the velocity patterns due to the buoyancy-induced secondary flows.

Velocity in the y-direction, represented with  $v$ , has the dominant impact on the average velocity compared to  $u$  and  $w$ . As shown in Fig. 5b, the air velocity in this direction increases along the channel from bottom to top. The local  $v$  distribution in the inter-fin gap shows a definite decline in magnitude as the inclination angle rises. The drop in velocity results in a reduction in the heat transfer coefficient within the inter-fin gap. From the symmetric distribution of  $v$ , at  $\psi = 90^\circ$ , the same flow structure observed in Fig. 2f can be easily identified inside the channel. The air flows very weakly in the opposite direction to the y-axis in the first half, while it flows in the same direction as the y-axis in the second half.

It is clear from Fig. 5c that the  $w$  (velocity in the z-direction) is too low to contribute to convective heat transfer. The local  $w$  magnitude increases along the length of the heat sink, approaching a maximum value around  $y = 0.05$  m, then dropping steadily close to  $y = 0.2$  m before increasing again toward the exit. Whereas, from the  $0^\circ$  to  $80^\circ$  inclination angles, only cold air enters the inter-fin spacing. In the horizontally oriented heat sink, only the sections close to the bottom and top edge experience cold air entrance, and the mid-section experiences hot air exit.

### *Temperature field for sideways inclination*

The temperature distribution is tied to the velocity field in natural convection. Fig. 6 depicts the temperature profile in and around the heat sink at various orientation angles on the x-y plane. The observation plane is 5 mm above the fin base. Initially, the vertically-rising cold air enters into inclined channels from the bottom end and travels along them, then exiting vertically with increased temperature. The colder air coming from the bottom edge warms up, generating a rising plume of air. Given that buoyancy is the primary underlying force behind this phenomenon, a plume ascends against gravity regardless of the inclination angle. The average temperature rises as the angle increases, implying reduced heat transfer rates at greater inclination angles. Heat dissipation performance is seen to be the lowest at  $\psi=90^\circ$ , and it is observed to be primarily caused by an intensive blocking of the airflow (Fig. 4). Conduction through the fluid replaces convection as the major mechanism of heat transfer, resulting in a reduction in overall heat transfer from the fin array.

### *Variation of heat sink temperature and heat transfer rate with sideways inclination*

Predicting the rate of heat transfer is useful as it can provide the necessary information to enhance the functionality and design of a heat transfer device. Fig. 7 illustrates the average heat sink temperature ( $T_w$ ) and convective heat transfer rate ( $Q_c$ ) as a function of the inclination angle for all three fin heights. Based on this figure, the following observations can be made about the sideways inclinations of the heat sink:

- In the  $0^\circ$ - $30^\circ$  inclination angles,  $T_w$  and  $Q_c$  are nearly constant;
- $T_w$  and  $Q_c$  change steadily from  $30^\circ$  to  $90^\circ$ . The lower the angle, the better the thermal performance.  $Q_c$  from the horizontally oriented heat sink ( $\psi=90^\circ$ ) is significantly smaller than  $Q_c$  from the vertically oriented one ( $\psi=0^\circ$ ) and, as such, the  $90^\circ$ -orientation case

can cause the temperature to rise. Accordingly, it can be inferred that the heat sink installation angle has a significant inhibitory effect on heat transfer performance; and

- In between the sideways inclination angle range of  $80^\circ$  and  $90^\circ$ , the fin height plays an important role. Fins block the buoyancy-driven flow to enter the fin spacings as the fin length becomes perpendicular to the gravity vector. Therefore, in this specific range of inclination angles, the smaller the fin height, the less its blocking effect on the flow and, subsequently, a better heat transfer rate.

#### *Validity range of modified correlation*

Table 1 presents the range of the change related to the important parameters that directly influence the natural convection heat transfer rate from the heat sink at various angles of inclination for only  $Q_{in}=75W$ . Since the data for  $H=5$  mm exhibits a distinct distribution pattern compared to the other two fin heights, and also because the ratio of  $H/L=0.02$  is uncommon for a heat sink (resembling a flat plate) [2], the data are presented only for  $H=15$  and  $25$  mm in the table. The  $Gr'$  represents the relationship between buoyancy and the viscous force exerted on the air, and the variations in the density of the fluid caused by temperature gradients have a direct impact on its magnitude. Hence, the higher the heat input, the higher the surface temperature and the higher the  $Gr'Pr$  for all tested cases. Based on Eq. (21),  $Gr'$  is also proportional to two dimensionless ratios, namely  $S/H$  and  $H/L$ . Based on the table,  $Nu_s$  is higher for the cases where these ratios are lower. Moreover, the highest values for the  $Nu_s$  are reached when the heat sink is oriented vertically ( $\psi=0^\circ$ ). As the angle of inclination increases, the  $Nu_s$  continuously decreases.

The plot of  $Nu_s$  versus  $Gr'Pr$  is shown in Fig. 8. Accordingly, as the inclination angle increases,  $Nu_s$  decreases. At all values of  $Gr'Pr$ , the rate of  $Nu_s$  decline rises as the inclination angle increases. It is expected that by replotting  $Nu_s$  as a function of  $Gr'Pr \cos(\psi)$ , the amount

by which the heat sink inclination reduces  $Nu_s$  can be determined. In correlations representing free convection from inclined plates, this change to the independent variable,  $Gr'Pr$ , is commonly utilized. A cosine correction of up to  $80^\circ$  was recommended in [15,25] for inclined channels. The premise behind this method is that the flow structure remains unchanged, with the only difference being in the body force. The validity of this correction on plate-fin heat sink correlations has not been studied extensively. However, it is expected that, since the flow field is assumed fully developed and the flow structure remains nearly unchanged for  $0^\circ \leq \psi \leq 80^\circ$ , the inclination impact on the  $Gr'Pr$  value should be proportional to the cosine of the degree of tilt angle [26]. Therefore, the correlation suggested in Eq. (23) can be modified by multiplying  $Gr'Pr$  with  $\cos(\psi)$  to obtain a correlation suitable for the sideways-inclined heat sink as:

$$Nu_s = 0.252(Gr'Pr \cos \psi)^{1/3} \quad \text{for } 250 < Gr'Pr < 10^6, H \geq 15 \text{ mm}, 0^\circ \leq \psi \leq 80^\circ \quad (24)$$

Observations show that when the inclination angle is in the  $80^\circ$  to  $90^\circ$  range, heated air is forced out mostly through the open surface rather than the top edge, as seen in Fig. 2f. Therefore, the cosine correction for the vertical correlation does not appear to be valid for these inclination angles that deviate considerably from the vertical position as a result of a significant change in the flow structure and strong secondary flows attributed to the mixing and vortices. As seen in Fig. 8, the data for this range of inclination angles are more distant from the others.

Fig. 9 illustrates  $Nu_s$  as a function of the new independent variable,  $Gr'Pr \cos(\psi)$ , for inclination angles only in the range of  $0^\circ \leq \psi \leq 80^\circ$ . All data collapse into a single curve with no discernible scattering, demonstrating the efficacy of this parameter. This wide range of application of the inclination angles for the present study, compared to the flat plates, is attributed to the finned surface, which maintains a 2D flow structure in the channels.

Statistical analysis of the simulation results is done using the standard least squares approach, and the deviations from the fit are computed. Since all the power fits are non-linear, the following formula is used to determine the coefficient of determination,  $R^2$ , which represents the quality of the fit:

$$R^2 = 1 - \frac{\sum(y - \hat{y})^2}{\sum(y - \bar{y})^2} \quad (25)$$

where  $y$  is the observed value in the dataset,  $\hat{y}$  is the predicted value from the regression model, and  $\bar{y}$  is the average of  $y$ . The  $R^2$  value for the curve fit is 0.951. When compared to the stated accuracy for similar correlations in the literature, Eq. (24) can be deemed highly accurate.

#### *Correlation for 3D inclination*

Understanding the impact of various inclination angles, including pitch, roll, or their combinations, on the flow and thermal characteristics of natural convection from plate-fin heat sinks is of significant interest. Moreover, it is essential to ascertain whether the proposed correlation remains applicable across different scenarios. The insights gained from this study can serve as valuable guidance for the thermal management design of systems resembling solar panels, especially when subjected to varying orientations during operation. To address this, the considered model is simulated at various combinational orientations including six different pitch angles ( $\theta = -30^\circ, -45^\circ, -60^\circ, 30^\circ, 45^\circ, \text{ and } 60^\circ$ ) along with three different roll angles ( $\psi = 30^\circ, 45^\circ, \text{ and } 60^\circ$ ), resulting in a total of eighteen simulation cases. The negative values for pitch angles represent the backward inclination. The proposed correlation, which incorporates both pitch and roll angles, is expressed as:

$$\text{Nu}_s = 0.252(\text{Gr}' \text{Pr} \cos \theta \cos \psi)^{1/3} \quad \text{for} \quad \begin{array}{l} 250 < \text{Gr}'\text{Pr} < 10^6, H \geq 15 \text{ mm}, \\ -60^\circ \leq \theta \leq 80^\circ, 0^\circ \leq \psi \leq 80^\circ \end{array} \quad (26)$$

Examining the simulation results alongside the modified correlation in Fig. 10 reveals a strong level of agreement, quantified by  $R^2 = 0.925$ . This robust correlation underscores its potential utility in estimating heat transfer rates from plate-fin heat sinks across a spectrum of orientations. The comprehensive nature of our investigation and the validation of the proposed correlation enhance our understanding of natural convection phenomena and offer practical insights for thermal management design considerations.

## Conclusion

This study examines the behavior of velocity and temperature contours as a function of sideways-inclination angles, providing fundamental scientific insight into plate-fin heat sink performance. Our findings indicate that small inclinations have little impact on heat transfer rate, while greater inclination angles reduce heat dissipation effectiveness. Secondary flow structures emerge at inclination angles between  $80^\circ$  to  $90^\circ$ , transitioning the flow regime from two-dimensional to three-dimensional vortex rolls. Increasing fin height obstructs cool air introduction into inter-fin channels, adversely affecting heat transfer performance. From  $0^\circ$  to  $80^\circ$  inclinations, variations in velocity components are not significant, maintaining a similar flow configuration through the channels between the fins. Thus, within this range, the effective body force remains  $\rho g \cos(\psi)$  and the modified vertical case correlation holds true. The correlation between  $Nu_s$  and  $Gr'Pr$  demonstrates good agreement with simulation results, with lower  $S/H$  and  $H/L$  ratios improving both  $Gr'$  and  $Nu_s$ . The suggested correlation for 3D inclination matches well with simulation data, offering valuable insights for practical applications.

## Nomenclature

$c_p$  specific heat at constant pressure, (J/kg·K)

$C$  coefficient

$g$  gravitational acceleration,  $\text{m/s}^2$

$Gr$  Grashof number

$Gr'$  modified Grashof number

$h$  average heat transfer coefficient,  $\text{W}/(\text{m}^2 \cdot \text{K})$

$H$  fin height, mm

$k$  thermal conductivity of the air,  $\text{W}/(\text{m} \cdot \text{K})$

$L$  fin length, mm

$m_1, m_2$  power indices

$n$  power index

$Nu_s$  average Nusselt number based on fin spacing

$p$  pressure, Pa

$P$  non-dimensional pressure

$Pr$  Prandtl number

$Q_c$  convection heat transfer rate from fin array, W

$Q_{in}$  power supplied to the heater plate, W

$Q_r$  radiative heat transfer rate from fin array, W

$R^2$  coefficient of determination

$S$  fin spacing, mm

$S_{opt}$  optimum fin spacing, mm

$T$  temperature,  $^{\circ}\text{C}$

$T_w$  average heat sink temperature,  $^{\circ}\text{C}$

$T_a$  ambient temperature,  $^{\circ}\text{C}$

$\Delta T$  surface-to-ambient temperature difference, °C

$u, v, w$  velocities in  $x, y$  and  $z$  directions, m/s

$u', v'$  characteristic velocities in  $x$  and  $y$  directions

$\mathcal{U}, \mathcal{V}$  non-dimensional velocities in  $x$  and  $y$  directions

$W$  heat sink width, mm

$x, y, z$  Cartesian coordinates

$X, Y, Z$  Non-dimensional coordinates

$y$  observed value in the dataset

$\bar{y}$  average of observed values

$\hat{y}$  predicted value from the regression model

*Greek symbols*

$\beta$  volumetric thermal expansion coefficient, 1/K

$\mu$  dynamic viscosity, Pa·s

$\nu$  kinematic viscosity, m<sup>2</sup>/s

$\rho$  density, kg/m<sup>3</sup>

$\theta$  backward or forward inclination angle (pitch angle), degrees

$\psi$  sideways inclination angle (roll angle), degrees

$\phi$  non-dimensional temperature

## **Acknowledgment**

The author gratefully appreciates Prof. Dr. Ilker Tari for the original suggestion for this area of investigation.

## **References**

- [1] I. Tari and M. Mehrtash, "Natural convection heat transfer from inclined plate-fin heat sinks," *Int. J. Heat Mass Transfer*, vol. 56, no. 1–2, pp. 574–593, 2013. DOI: 10.1016/j.ijheatmasstransfer.2012.08.050.
- [2] M. Mehrtash and I. Tari, "A correlation for natural convection heat transfer from inclined plate-finned heat sinks," *Appl. Therm. Eng.*, vol. 51, no. 1–2, pp. 1067–1075, 2013. DOI: 10.1016/j.applthermaleng.2012.10.043.
- [3] I. Tari and M. Mehrtash, "Natural convection heat transfer from horizontal and slightly inclined plate-fin heat sinks," *Appl. Therm. Eng.*, vol. 61, no. 2, pp. 728–736, 2013. DOI: 10.1016/j.applthermaleng.2013.09.003.
- [4] I. Tari and F. S. Yalcin, "CFD analyses of a notebook computer thermal management system and a proposed passive cooling alternative," *IEEE Transactions on Components and Packaging Technologies*, vol. 33, no. 2, pp. 443–452, 2010. DOI: 10.1109/TCAPT.2010.2044505.
- [5] C. W. Leung and S. D. Probert, "Heat-exchanger performance: Effect of orientation," *Appl. Energy*, vol. 33, no. 4, pp. 235–252, 1989. DOI: 10.1016/0306-2619(89)90057-3.
- [6] I. Tari, "Passive cooling assembly for flat panel displays with integrated high power components," *IEEE Transactions on Consumer Electronics*, vol. 55, no. 3, pp. 1707–1713, 2009. DOI: 10.1109/TCE.2009.5278046.
- [7] Y. Huang, S. Shen, H. Li, and Y. Gu, "Numerical analysis on the thermal performances of different types of fin heat sink for high-power led lamp cooling," *Thermal Science*, vol. 23, no. 2A, pp. 625–636, 2019. DOI: 10.2298/tsci170623233h.

- [8] Q. Shen, D. Sun, Y. Xu, T. Jin, and X. Zhao, "Orientation effects on natural convection heat dissipation of rectangular fin heat sinks mounted on LEDs," *Int. J. Heat Mass Transfer*, vol. 75, pp. 462–469, 2014. DOI: 10.1016/j.ijheatmasstransfer.2014.03.085.
- [9] Z. Zhang, E. Lau, C. Botting, and M. Bahrami, "Naturally cooled heat sinks for battery chargers," *Int. J. Heat Mass Transfer*, vol. 147, p. 118911, 2020. DOI: 10.1016/j.ijheatmasstransfer.2019.118911.
- [10] G. E. Lau *et al.*, "Modelling of natural convection in vertical and tilted photovoltaic applications," *Energy Build.*, vol. 55, pp. 810–822, 2012. DOI: 10.1016/j.enbuild.2012.10.014.
- [11] C. G. Popovici, S. V. Hudişteanu, T. D. Mateescu, and N. C. Cherecheş, "Efficiency Improvement of Photovoltaic Panels by Using Air Cooled Heat Sinks," *Energy Procedia*, vol. 85, no. November 2015, pp. 425–432, 2016. DOI: 10.1016/j.egypro.2015.12.223.
- [12] E. Johnston, P. S. B. Szabo, and N. S. Bennett, "Cooling silicon photovoltaic cells using finned heat sinks and the effect of inclination angle," *Thermal Science and Engineering Progress*, vol. 23, no. March, p. 100902, 2021. DOI: 10.1016/j.tsep.2021.100902.
- [13] J. K. Tonui and Y. Tripanagnostopoulos, "Improved PV/T solar collectors with heat extraction by forced or natural air circulation," *Renew. Energy*, vol. 32, no. 4, pp. 623–637, 2007. DOI: 10.1016/j.renene.2006.03.006.
- [14] A. G. Straatman, D. Naylor, J. M. Floryan, and J. D. Tarasuk, "A Study of natural convection between inclined isothermal plates," *J. Heat Transfer*, vol. 116, no. 1, pp. 243–245, 1994. DOI: 10.1115/1.2910866.
- [15] O. Manca and S. Nardini, "Composite correlations for air natural convection in tilted channels," *Heat Transfer Engineering*, vol. 20, no. 3, pp. 64–72, 1999. DOI: 10.1080/014576399271439.

- [16] O. Manca and S. Nardini, “Thermal design of uniformly heated inclined channels in natural convection with and without radiative effects,” *Heat Transfer Engineering*, vol. 22, no. 2, pp. 13–28, 2001. DOI: 10.1080/014576301462227.
- [17] K. E. Starner and H. N. McManus, “An experimental investigation of free-convection heat transfer from rectangular-fin arrays,” *J. Heat Transfer*, vol. 85, no. 3, pp. 273–277, 1963. DOI: 10.1115/1.3686097.
- [18] G. Mittelman, A. Dayan, K. Dado-Turjeman, and A. Ullmann, “Laminar free convection underneath a downward facing inclined hot fin array,” *Int. J. Heat Mass Transfer*, vol. 50, no. 13–14, pp. 2582–2589, 2007. DOI: 10.1016/j.ijheatmasstransfer.2006.11.033.
- [19] B. Yazıcıoğlu, “Performance of rectangular fins on a vertical base in free convection heat transfer,” M.S. thesis, Dept. Mech. Eng., Middle East Technical University, Ankara, Turkey, 2005.
- [20] Q. Chen and W. Xu, “A zero-equation turbulence model for indoor airflow simulation,” *Energy Build.*, vol. 28, no. 2, pp. 137–144, 1998. DOI: 10.1016/s0378-7788(98)00020-6.
- [21] M. Mehrtash, “Numerical investigation of natural convection from inclined plate finned heat sinks,” M.S. thesis, Dept. Mech. Eng., Middle East Technical University, Ankara, Turkey, 2011.
- [22] C. W. Leung, S. D. Probert, and M. J. Shilston, “Heat exchanger design: Optimal uniform separation between rectangular fins protruding from a vertical rectangular base,” *Appl. Energy*, vol. 19, no. 4, pp. 287–299, 1985. DOI: 10.1016/0306-2619(85)90003-0.
- [23] C. W. Leung, S. D. Probert, and M. J. Shilston, “Heat exchanger: Optimal separation for vertical rectangular fins protruding from a vertical rectangular base,” *Appl. Energy*, vol. 19, no. 2, pp. 77–85, 1985. DOI: 10.1016/0306-2619(85)90063-7.

- [24] C. W. Leung and S. D. Probert, "Thermal effectiveness of short-protrusion rectangular, heat-exchanger fins," *Appl. Energy*, vol. 34, no. 1, pp. 1–8, 1989. DOI: 10.1016/0306-2619(89)90050-0.
- [25] S. A. M. Said, M. A. Habib, H. M. Badr, and S. Anwar, "Numerical investigation of natural convection inside an inclined parallel-walled channel," *Int. J. Numer. Methods Fluids*, vol. 49, no. 5, pp. 569–582, 2005. DOI: 10.1002/flid.1013.
- [26] A. Hajji and W. M. Worek, "Analysis of combined fully-developed natural convection heat and mass transfer between two inclined parallel plates," *Int. J. Heat Mass Transfer*, vol. 31, no. 9, pp. 1933–1940, 1988. DOI: 10.1016/0017-9310(88)90206-2.

Table 1. Range of simulation data.

$\psi$ (°)	$S/H$	$H/L$	$Q_{in}$ (W)	$Q_c$ (W)	$Q_r$ (W)	$T_w$ (°C)	Gr'Pr	Gr'Pr $\cos(\psi)$	Nu <sub>s</sub>
0	0.0783	0.06	75	55.01	9.96	80.3	1205.52	1205.52	2.68
	0.47	0.1	75	57.87	9.29	67.9	812.07	812.07	2.48
10	0.0783	0.06	75	55	10	80.5	1207.5	1189.155	2.67
	0.47	0.1	75	57.83	9.32	68.038	813.29	800.9343	2.47
20	0.0783	0.06	75	54.8	10.1	80.87	1211.9	1138.813	2.65
	0.47	0.1	75	57.7	9.4	68.41	817.28	767.992	2.45
30	0.0783	0.06	75	54.53	10.24	81.6	1220	1056.551	2.6
	0.47	0.1	75	57.42	9.58	69.12	825	714.471	2.4
45	0.0783	0.06	75	53.71	10.7	83.7	1242.87	878.8418	2.47
	0.47	0.1	75	56.6	10.08	71.8	846.7	598.7073	2.26
60	0.0783	0.06	75	52.13	11.6	87.64	1283.55	641.775	2.25
	0.47	0.1	75	54.94	11.06	75.1	885.6	442.8	2.03
70	0.0783	0.06	75	49.2	13.22	94.62	1348.75	461.2997	1.97
	0.47	0.1	75	52.95	12.25	79.63	927.83	317.3365	1.81
80	0.0783	0.06	75	45.81	15.1	102.1	1379.47	239.5419	1.76
	0.47	0.1	75	49.35	14.41	87.51	993.21	172.4691	1.47
90	0.0783	0.06	75	44.5	15.79	104.83	1429.91	-	1.46
	0.47	0.1	75	43.57	17.9	99.21	1074.5	-	1.08

## Figure captions

Fig. 1. a) The computational domain; b) Exploded view of the assembly; c) Illustration of pitch-and-roll inclination angles along with geometrical dimensions of the heat sink; and d) Heat sink view in vertical ( $\psi = 0^\circ$ ) and horizontal ( $\psi = 90^\circ$ ) orientations for sideways inclination.

Fig. 2. The streamlines for a) the vertical ( $\psi = 0^\circ$ ) and sideways-inclined heat sinks at b)  $30^\circ$ , c)  $45^\circ$ , d)  $70^\circ$ , e)  $80^\circ$ , and f)  $90^\circ$  for  $Q_{in}=75$  W and  $H=25$  mm.

Fig. 3. The velocity vectors inside the middle channel of the heat sink for a) the vertical ( $\psi = 0^\circ$ ) and sideways-inclined cases at b)  $30^\circ$ , c)  $45^\circ$ , d)  $70^\circ$ , e)  $80^\circ$ , and f)  $90^\circ$  for  $Q_{in}=75$  W and  $H=25$  mm.

Fig. 4. The secondary flow in between the horizontal fins on a vertical base at  $Q_{in} =75$  W for fin heights of a)  $H=5$  mm, b)  $H=15$  mm, c)  $H=25$  mm.

Fig. 5. The changes of a)  $u$ , b)  $v$ , and c)  $w$  in the middle channel along the fin length for different inclination angles.

Fig. 6. The temperature contours for a) the vertical ( $\psi = 0^\circ$ ) and sideways-inclined heat sinks at b)  $30^\circ$ , c)  $45^\circ$ , d)  $70^\circ$ , e)  $80^\circ$ , and f)  $90^\circ$  for  $Q_{in}=75$  W and  $H=25$  mm.

Fig. 7. a) The change of heat sink temperature as a function of inclination angle; b) The change of convection heat transfer rate as a function of inclination angle.

Fig. 8.  $Nu_s$  versus  $Gr'Pr$  in all sideways inclination angles for  $H=15$  and  $25$  mm.

Fig. 9. The curve fit of the simulation results for inclination angles in the  $0^\circ$ - $80^\circ$  range concerning  $H=15$  mm and  $H=25$  mm.

Fig. 10. The comparison of the proposed correlation for 3D inclination and the data obtained from the simulations for various orientations of the plate-fin heat sink.

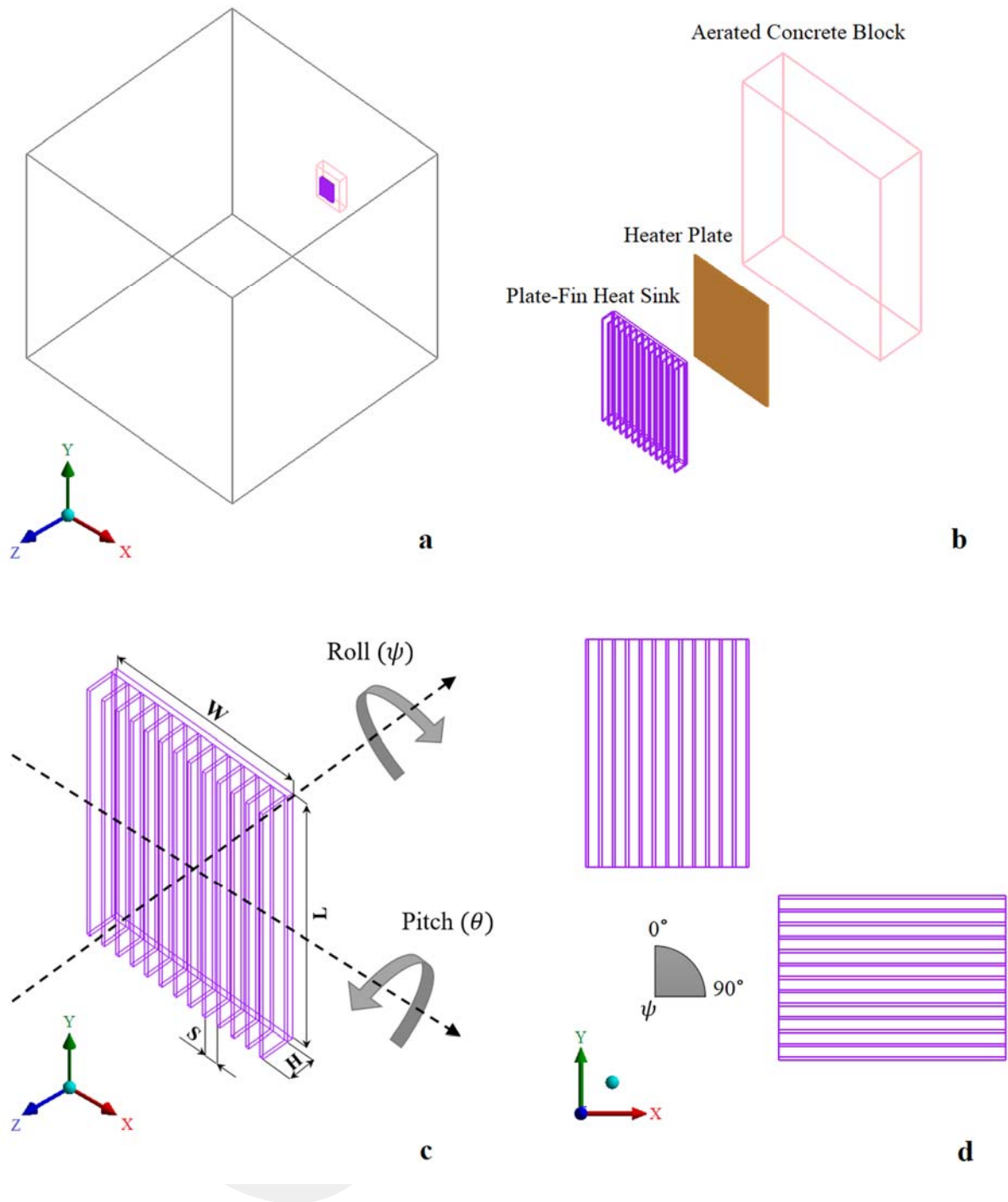


Fig. 1. a) The computational domain; b) Exploded view of the assembly; c) Illustration of pitch-and-roll inclination angles along with geometrical dimensions of the heat sink; and d) Heat sink view in vertical ( $\psi = 0^\circ$ ) and horizontal ( $\psi = 90^\circ$ ) orientations for sideways inclination.

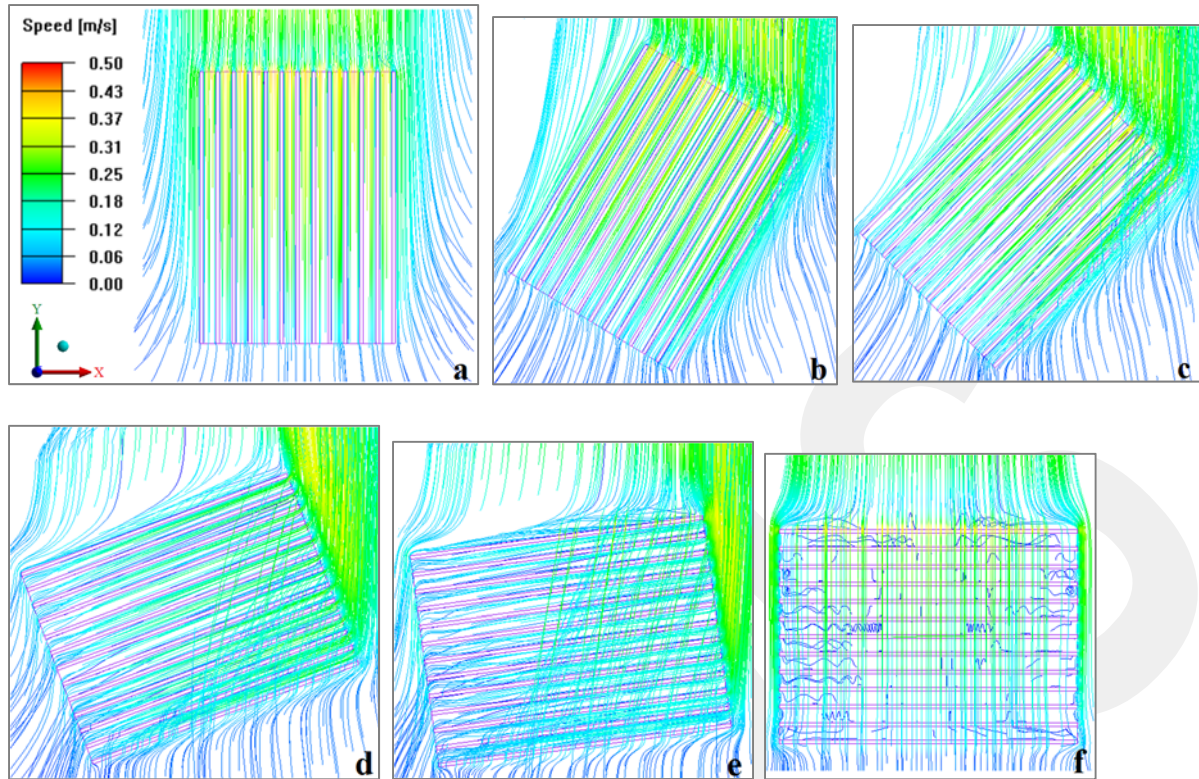


Fig. 2. The streamlines for a) the vertical ( $\psi = 0^\circ$ ) and sideways-inclined heat sinks at b)  $30^\circ$ , c)  $45^\circ$ , d)  $70^\circ$ , e)  $80^\circ$ , and f)  $90^\circ$  for  $Q_{in}=75$  W and  $H=25$  mm.

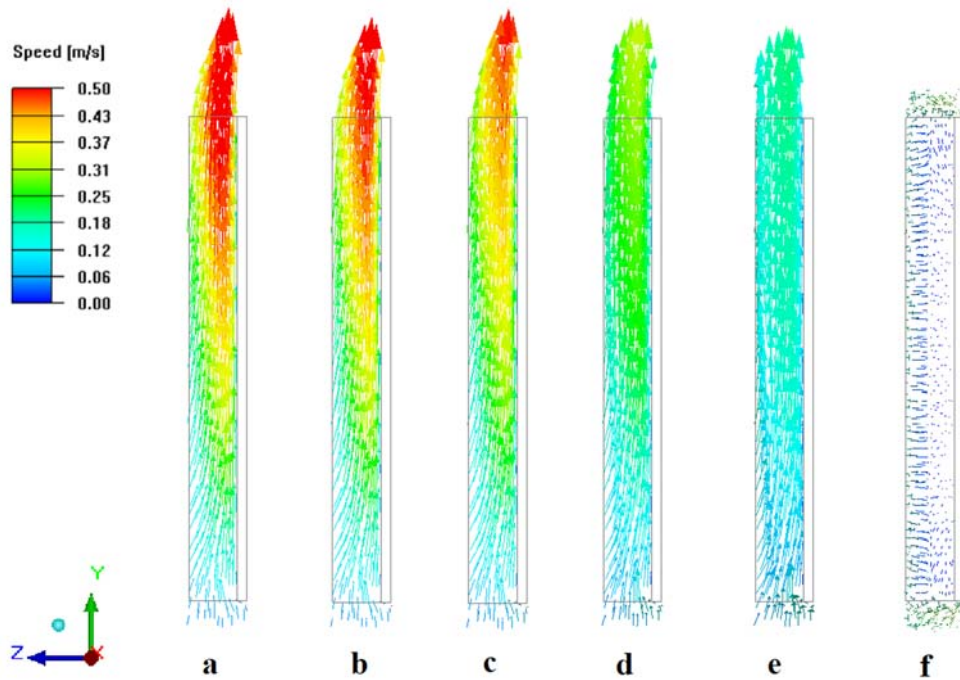


Fig. 3. The velocity vectors inside the middle channel of the heat sink for a) the vertical ( $\psi = 0^\circ$ ) and sideways-inclined cases at b)  $30^\circ$ , c)  $45^\circ$ , d)  $70^\circ$ , e)  $80^\circ$ , and f)  $90^\circ$  for  $Q_{in}=75$  W and  $H=25$  mm.

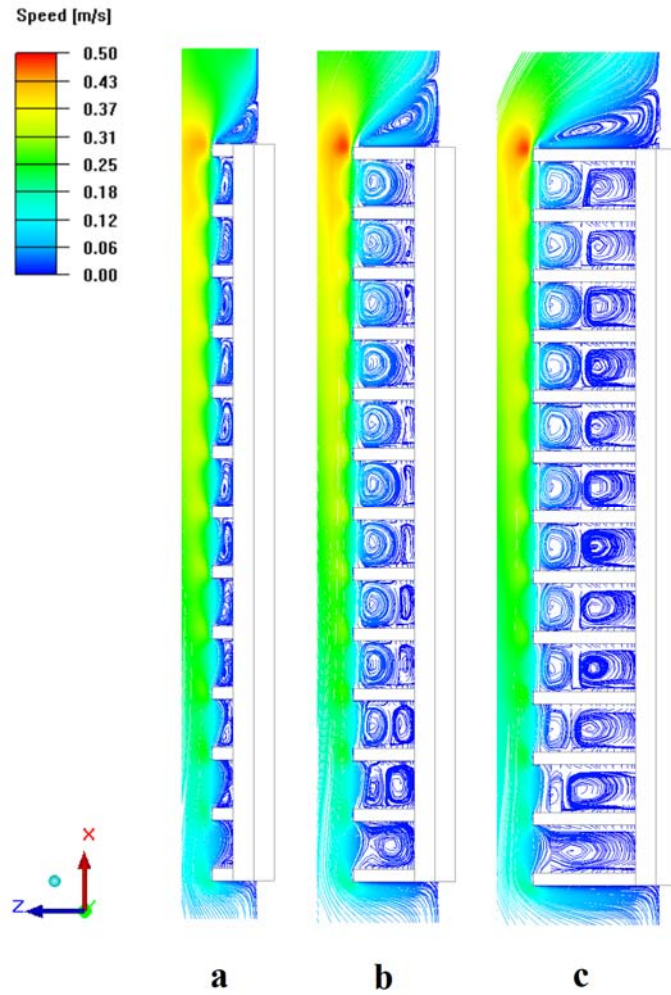
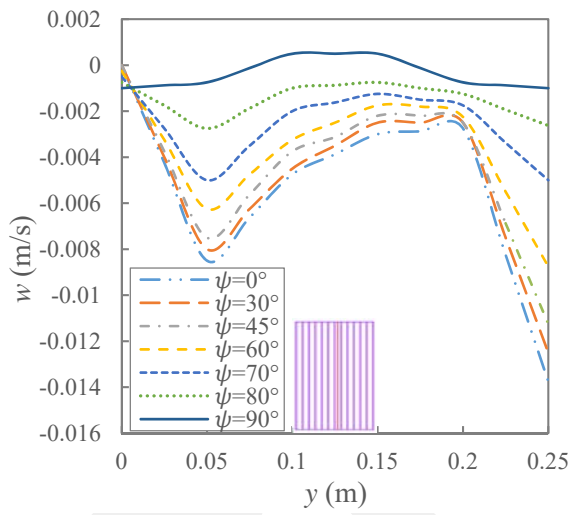
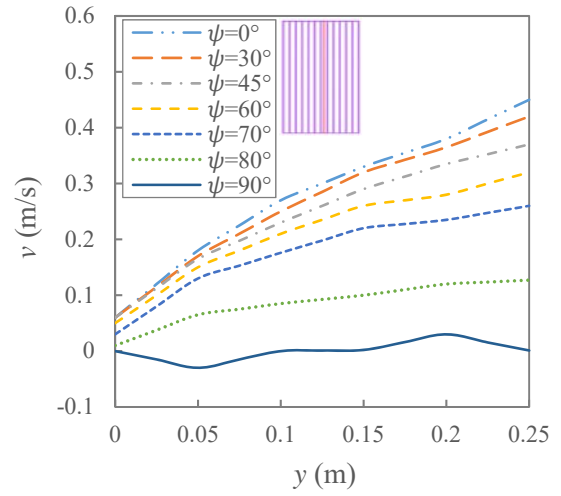
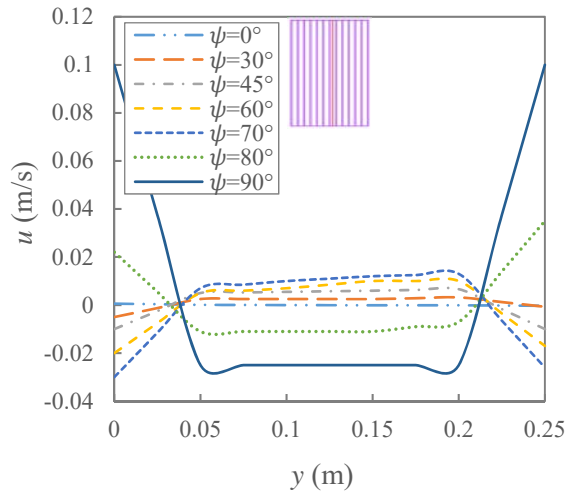


Fig. 4. The secondary flow in between the horizontal fins on a vertical base at  $Q_{in} = 75$  W for fin heights of a)  $H=5$  mm, b)  $H=15$  mm, c)  $H=25$  mm.



**a**

**b**

**c**

Fig. 5. The changes of a)  $u$ , b)  $v$ , and c)  $w$  in the middle channel along the fin length for different inclination angles.

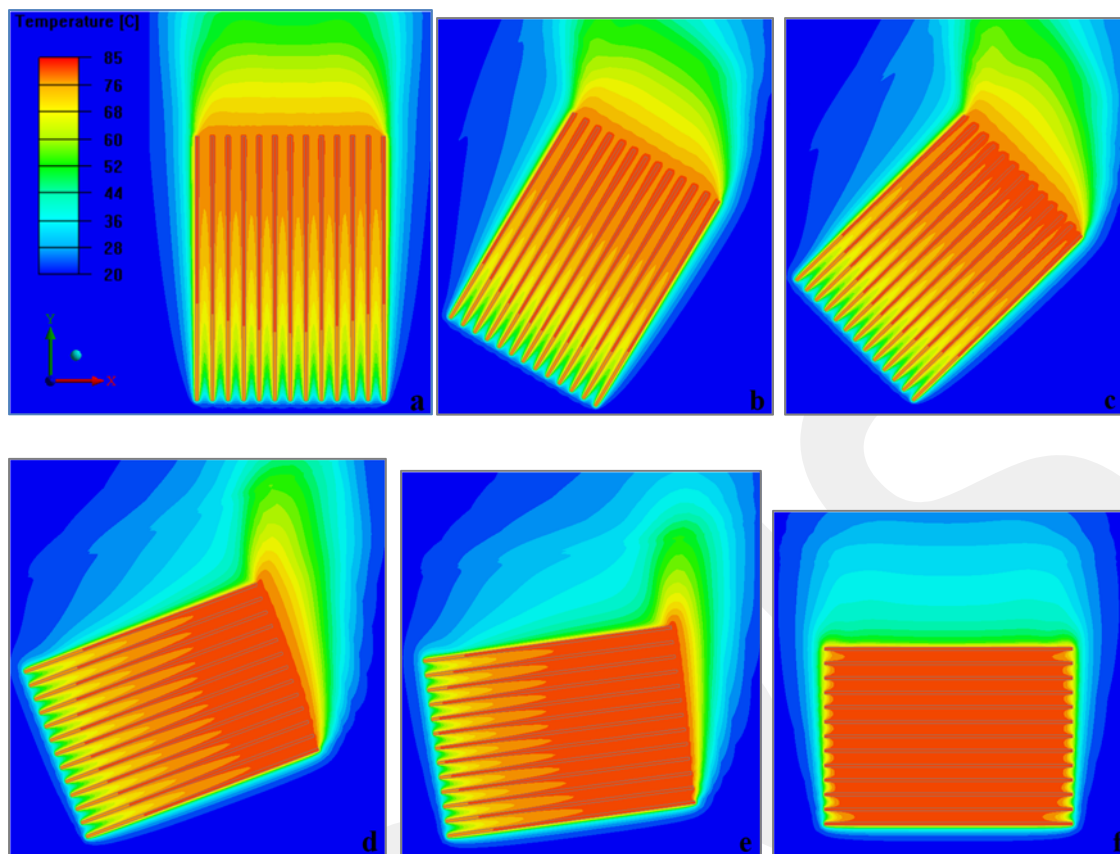


Fig. 6. The temperature contours for a) the vertical ( $\psi = 0^\circ$ ) and sideways-inclined heat sinks at b)  $30^\circ$ , c)  $45^\circ$ , d)  $70^\circ$ , e)  $80^\circ$ , and f)  $90^\circ$  for  $Q_{in}=75$  W and  $H=25$  mm.

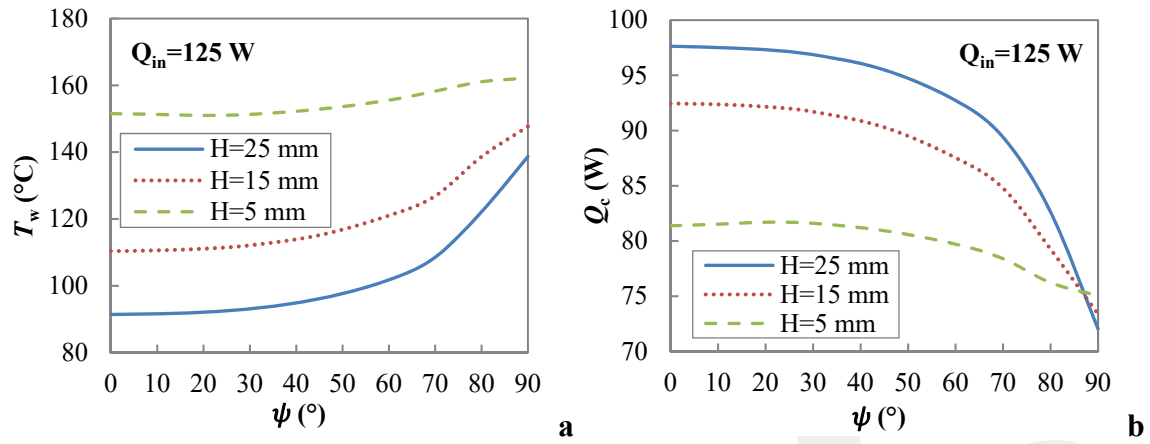


Fig. 7. a) The change of heat sink temperature as a function of inclination angle; b) The change of convection heat transfer rate as a function of inclination angle.

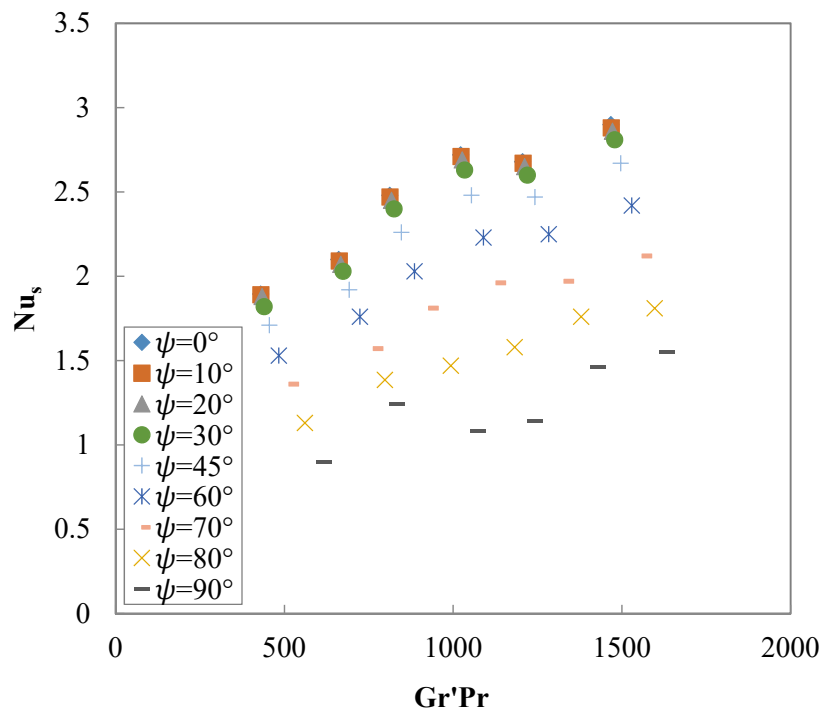


Fig. 8.  $Nu_s$  versus  $Gr'Pr$  in all sideways inclination angles for  $H=15$  and  $25$  mm.

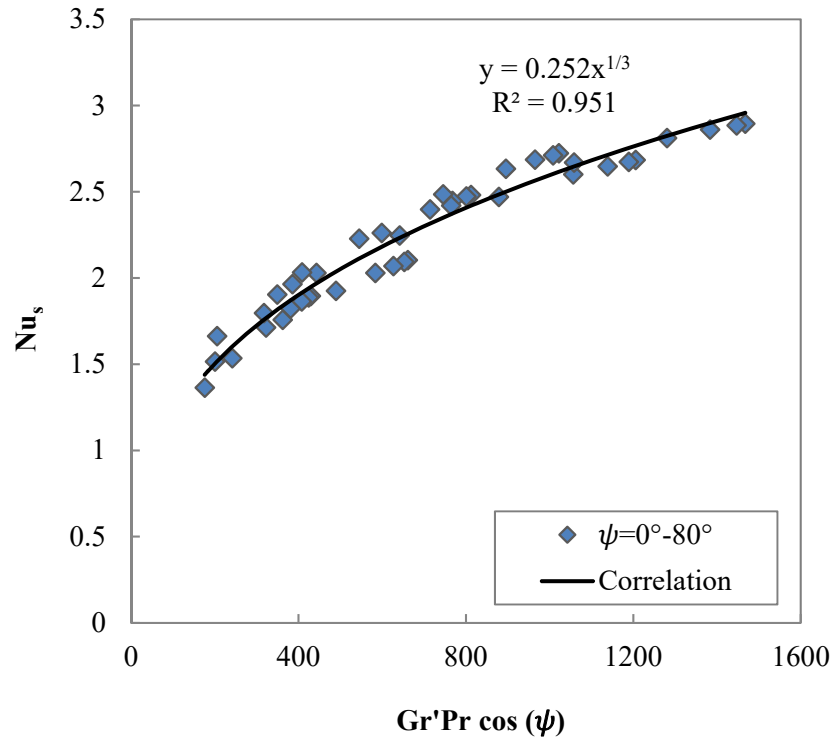


Fig. 9. The curve fit of the simulation results for inclination angles in the  $0^\circ$ - $80^\circ$  range concerning  $H=15$  mm and  $H=25$  mm.

$\theta$ (°)	-30	-45	-60	30	45	60
$\psi$ (°)	30	30	30	30	30	30
	45	45	45	45	45	45
	60	60	60	60	60	60

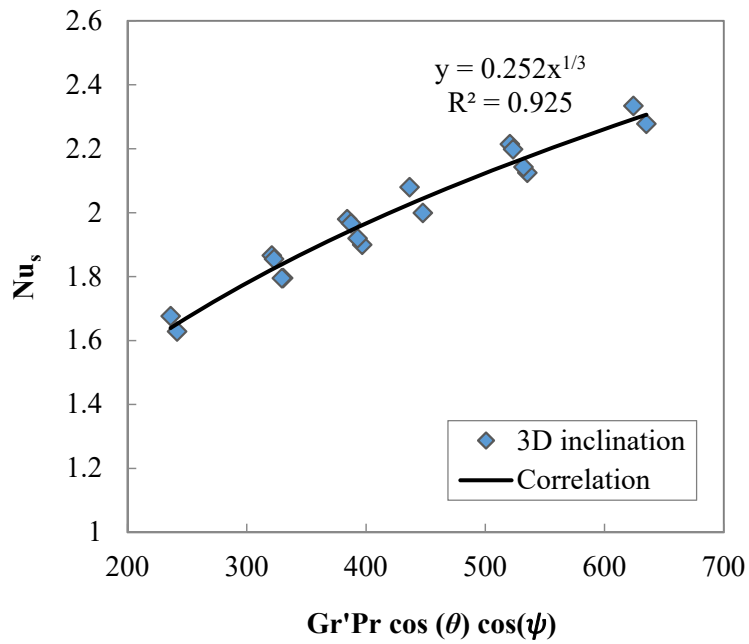


Fig. 10. The comparison of the proposed correlation for 3D inclination and the data obtained from the simulations for various orientations of the plate-fin heat sink.



**Mehdi Mehrdash** is an assistant professor of Energy Systems Engineering at Atilim University. He holds a BS in Mechanical Engineering from Urmia University and an MS and PhD in Mechanical Engineering from Middle East Technical University (METU). His research areas include electronics cooling, computational fluid dynamics, fuel cells, solar energy, and thermal energy storage.

Journal Name: Heat Transfer Engineering

DOI Number: [10.1080/01457632.2024.2407668](https://doi.org/10.1080/01457632.2024.2407668)